

Quantum Event Identification and Simulation of Quantum Event-Learning Procedures

Chun-Yuan Hsu

National Tsing Hua University

chunyuan.hsu.me@gapp.nthu.edu.tw

Han-Hsuan Lin

National Tsing Hua University

linhh@cs.nthu.edu.tw

June 14, 2025

Abstract

Quantum state tomography is a central task in quantum information science, but it typically requires a prohibitively large number of samples that scale poorly with system dimension. This challenge has motivated the exploration of more efficient quantum learning problems that avoid full state reconstruction. One of such problems is shadow tomography introduced by Scott Aaronson [1], which requires the estimations of the shadow, a given set of two-outcome measurements. Consequently, when the number of shadows are not too large, shadow tomography was shown to be solvable in exponentially lower sample complexity compared to full quantum state tomography. Inspired by shadow tomography, we introduce the Quantum Event Identification (QEI) problem, which targets identifying measurements with high success rates while requiring fewer samples. Unlike standard shadow tomography, which focuses on obtaining global accuracy across all observables, QEI emphasizes per-measurement success. Exploiting a promised gap in acceptance probabilities, QEI can potentially achieve lower sample complexity compared to shadow tomography. We evaluate the complexity of QEI through simulations of various measurement procedures inspired by procedures of quantum event finding introduced by Adam Bene Watts and John Bostanci [2]. These procedures achieve stable success rates of around 60% with only a single copy of the unknown state in low-dimensional settings. We also adapt classical shadow and related techniques to QEI, examining their relative strengths and validating the event-finding bounds introduced in Section 1.4. Our results highlight the potential of QEI as a resource-efficient strategy for quantum measurement prediction, suggesting avenues for theoretical refinements and more scalable computational methods.

Keywords: Quantum Event Identification, Quantum Measurements, Blended Measurements, Classical Shadows, Simulation

1 Introduction

Quantum computers have the potential to outperform classical computers in specific problems because qubits can store information beyond a simple 0 or 1. However, due to the collapsing nature of quantum state measurement, we cannot directly retrieve all information from a unknown quantum state [3]. This fact has led to researches in quantum information science aimed at learning quantum states.

Quantum state tomography has been developed as a method to recover the full description of a unknown quantum state with several copies of the state [4–8]. It has been shown that, for a quantum state $\rho \in \mathbb{C}^{d \times d}$, $\Theta(d^2/\epsilon^2)$ copies is required to complete quantum state tomography with high success probability and precision ϵ in trace distance [9]. However, since the sample and time complexity of quantum state tomography

grows exponentially with number of qubits in the system, implementing quantum state tomography on large quantum systems is usually impractical.

In pursuit of more efficient methods of information extraction from quantum states, in 2018, Scott Aaronson proposed shadow tomography of quantum states [1].

Problem 1.1 (Shadow Tomography, Problem 1 from [1]). *given an unknown d -dimensional quantum mixed state ρ , as well as known two-outcome measurements M_1, \dots, M_m , each of which accepts ρ with probability $\text{Tr}[M_i\rho]$ and rejects ρ with probability $1 - \text{Tr}[M_i\rho]$, output numbers $b_1, \dots, b_m \in [0, 1]$ such that $\|b_i - \text{Tr}[M_i\rho]\| \leq \epsilon$ for all i . with success probability at least $1 - \epsilon$. Do this via a measurement of $\rho^{\otimes k}$, where $k = k(d, m, \epsilon, \delta)$ is as small as possible.*

Shadow tomography aims to address the scalability issues of quantum state tomography by waiving the need to get full information of the state. Instead, shadow tomography focuses on obtaining specific “shadows”, which are estimation of the two-outcomes measurements. In [1], Scott Aaronson constructed a procedure solving shadow tomography using $\tilde{O}(\log(1/\delta) \cdot \epsilon^{-4} \cdot \log^4 m \cdot \log d)^1$ copies of the unknown state. While the sample complexity only grows logarithmically with the system dimension d , it depends on m , the number of shadows.

Following Scott Aaronson’s result, in 2020, Huang, Kueng, and Preskill introduced classical shadow [10] as a process for shadow tomography where the measurement on the unknown state does not depend on the two-outcome measurements to be predicted. The classical shadow procedure employs randomized measurements on the unknown quantum state to create a “classical shadow,”² which approximates the unknown quantum state. “Classical shadow” is an array of matrices, containing N independent classical snapshots of the quantum state ρ . Specifically,

$$S(\rho; N) = \{\hat{\rho}_1, \hat{\rho}_2, \dots, \hat{\rho}_N\}, \quad \hat{\rho}_i = \mathcal{M}^{-1}(U_i^\dagger |b_i\rangle\langle b_i| U_i),$$

where $\{U_i\}$ are random unitaries from some ensemble to change the measurement basis, $\{|b_i\rangle\}$ are measurement outcomes, and \mathcal{M}^{-1} is the inverted quantum channel applied during post-processing. This array serves as a description of the quantum state, enabling efficient prediction of linear properties. The classical shadow procedure can be used to solve the shadow tomography problem by using the classical shadow array repeatedly to compute the expectation values of each two-outcome measurement one by one.

However, the number of sample needed for classical shadow to solve shadow tomography scales with the “shadow norm” of the two-outcome measurements. In particular, classical shadows of size N suffice to predict m arbitrary linear target functions $\text{Tr}[M_i\rho], \dots, \text{Tr}[M_m\rho]$ up to additive error ϵ , provided that

$$N = O\left(\log m \cdot \epsilon^{-2} \cdot \max_i \|M_i\|_{\text{shadow}}^2\right).$$

, where $\|M_i\|_{\text{shadow}}$ is the shadow norm. The shadow norm depends on the ensemble of random measurement used. For random Clifford measurements, shadow norm is equivalent to Hilbert–Schmidt norms, $\text{Tr}[M_i^2]$. Measurements with higher rank typically have larger Hilbert–Schmidt norms because $\text{Tr}[M_i^2]$ sums the squares of all eigenvalues of M_i . Consequently, the shadow norm of M_i can be as large as the dimension of the system, which significantly increases the sample complexity N . This makes accurate predictions computationally expensive for high-rank observables.

In 2020, Costin Badescu and Ryan O’Donnell proposed an algorithm to solve the quantum threshold search problem 1.2 in [11] using $O((\log^2 m)/\epsilon^2)$ samples. Moreover, they use their threshold search

¹ \tilde{O} hides a poly $(\log \log M, \log \log D, \log \epsilon^{-1})$ factor.

²“Classical shadow” is a overloaded name in [10], in which “classical shadow” implies both the procedure and the classical description of a unknown state.

algorithm to solve the shadow tomography problem with only $\tilde{O}((\log^2 m)(\log d)(\epsilon^{-4}))^3$ copies, achieving the best known dependence on the three parameters m , d , and ϵ .

Problem 1.2 (Quantum Threshold Search Problem, [11]). *Given:*

1. *Parameters* $0 < \epsilon, \delta < \frac{1}{2}$.
2. *Access to unentangled copies of an unknown d -dimensional quantum state ρ .*
3. *A list of d -dimensional observables $0 \leq M_1, \dots, M_m \leq \mathbb{I}$.*
4. *A list of thresholds $0 \leq \theta_1, \dots, \theta_m \leq 1$.*

The algorithm should either output:

- “ $\text{Tr}[M_j \rho] > \theta_j - \epsilon$ ” for some particular j ; or else,
- “ $\text{Tr}[M_i \rho] \leq \theta_i$ for all i ”.

The output of the algorithm is a sample from a distribution over indices j such that “ $\text{Tr}[M_j \rho] > \theta_j - \epsilon$ ” or “ $\text{Tr}[M_i \rho] \leq \theta_i$ for all i ” if no such j exists. The task is to minimize the number k of copies that are used, while ensuring the probability of a false output statement is at most δ .

Beside the quantum threshold search problem, Quantum OR Problem is another well-studied problem related to shadow tomography [12, 13].

Problem 1.3 (Quantum OR Problem, Theorem 26 from [2]). *Let $\mathcal{M} = \{M_1, M_2, \dots, M_m\}$ be a set of two-outcome measurements, and let ρ be an unknown quantum state. The goal of the OR problem is to distinguish the two cases:*

1. *There exists a measurement M_j that $\text{Tr}[M_j \rho] \geq \theta$ is high.*
2. *The total accepting probability of all measurements $\sum_i \text{Tr}[M_i \rho]$ is low.*

In [13], Scott Aaronson attempted to solve Quantum OR Problem using the random measurement method. However, his proof was later found to contain a flaw, as it failed to rule out the Anti-Zeno effect, as highlighted in [12].

Subsequently, in 2023, Adam Bene Watt and John Bostanci demonstrated in the paper “Quantum Event Learning and Gentle Random Measurement” [2] that the random measurement causes minimal disturbance on average. Consequently, they were able to rule out the occurrence of the Anti-Zeno effect in the random measurement method. Further, they demonstrate that the original Aaronson’s quantum OR algorithm, with minor modifications in the number of random measurements applied, remains valid. Furthermore, the authors propose their own procedure for the quantum OR problem, blended measurement, and demonstrate that its efficiency surpasses that of random measurement.

The authors of [2] also introduce a class of learning problems, “Event Learning,” which encompasses problems involving an unknown quantum state ρ and a set of measurements M_1, M_2, \dots, M_m , with the objective of learning properties of the measurements’ acceptance probabilities. Shadow tomography is identified as a specific instance of an Event Learning problem. Additionally, they introduces another Event Learning problems- Quantum Event Finding.

Problem 1.4 (Event Finding, [2]). *Let $\mathcal{M} = \{M_1, M_2, \dots, M_m\}$ be a set of two-outcome measurements, and let ρ be a quantum state such that either:*

³ \tilde{O} hides a poly factor $L = \log\left(\frac{\log d}{\delta \epsilon}\right)$.

- *There exists an $i \in [m]$ such that $\text{Tr}[M_i\rho] > 1 - \epsilon$ (Case 1), or*
- *$\sum_i \text{Tr}[M_i\rho] \leq \delta$ (Case 2).*

If the event is Case 1, the goal is to point out a measurement M_i with a large value of $\text{Tr}[M_i\rho]$. Conversely, in Case 2, the objective is to confirm that the event is Case 2.

Event Finding is similar to the quantum threshold search problem and the quantum OR problem. The first difference between Event Finding and threshold search is that event finding has only one “threshold probability” across all measurements. Additionally, event finding imposes a promise on its measurement set: the sum of the accepting probabilities for Case 2 must be less than or equal to δ . In contrast, in the quantum threshold search problem, if the measurements do not satisfy “case 1”, they must satisfy “case 2”. Compared to the quantum OR problem, Event Finding is a generalization. Event finding is more challenging because it not only requires discerning the event (Case 1 or Case 2) but also finding a measurement that accepts in Case 1.

In the latter part of [2], the authors adapt their measurement procedures to the quantum threshold search problem, achieving the same sample complexity, $O((\log^2 m)/\epsilon^2)$, as established in [11]. Similarly, they apply their algorithms to shadow tomography problem, attaining results that match the current best-known sample complexity of $\tilde{O}((\log^2 m)(\log d)/\epsilon^4)$.

1.1 Quantum Event Identification

In this work, we introduce the Quantum Event Identification (QEI) problem to efficiently identify measurements with high acceptance probabilities. In this sections, we present the motivation, advantages, and potential of QEI as a quantum event learning problem with low sample complexity. Additionally, QEI captures the spirit of shadow tomography: learning useful properties from an approximate shadow of the state, enabling fast estimation of non-commuting measurements.

Problem 1.5 (Quantum Event Identification). *Given an unknown mixed state ρ and known two-outcome measurements M_1, \dots, M_m , assume that for each $i \in [m]$, we are promised that either $\text{Tr}(M_i\rho) \geq c_i$ or $\text{Tr}(M_i\rho) \leq c_i - \epsilon$. We want to determine which of these conditions holds for each $i \in [m]$ so that, for every i , we successfully predict either $\text{Tr}[M_i\rho] \leq c_i - \epsilon$ or $\text{Tr}[M_i\rho] \geq c_i$ with a probability at least $1 - \Delta$. Note that the success probability $1 - \Delta$ is the success probability for predicting a single $\text{Tr}[M_i\rho]$.*

One of the key distinctions between Quantum Event Identification and shadow tomography is that it emphasizes the success probability of predicting the condition for each single measurement, rather than requiring the success probability of predicting all measurements correctly at once.

One of the motivation of Quantum Event Identification is to study the sample complexity of predicting an unknown quantum state. To illustrate this point, we first give an exposition of the sample complexity of shadow tomography.

The best-known sample upper bound of shadow tomography is about $O((\log^2 m)/\epsilon^4)$, where m denotes the number of observables [10,11], while Aaronson’s initial work suggests a lower bound of $\Omega((\log m)/\epsilon^2)$ [1]. Determining the exact sample complexity remains an open question.

Putting extra constraints on shadow tomography problem can reduce its sample complexity. In particular, many of shadow tomography’s applications have a promised gap in the accept probabilities; for example, in [1], a quantum one-way communication scenario is described in which Alice sends a quantum state $|\psi_x\rangle$ encoding information about x to Bob, who holds information about y in M_y and computes $f(x, y)$ for pairs $(x, y) \in S$, Bob then uses shadow tomography to estimate $\text{Tr}[M_y\psi_x]$ for all y . If we restrict to a total function f containing all (x, y) pairs, then there is a bounded probability gap within $\text{Tr}[M_y\psi_x]$, corresponding to the accept probability gap between $f = 0$ and $f = 1$. Additionally, quantum copy-protected software [1, 14]

uses a quantum state ρ_f to enable users to evaluate a Boolean function $f : \{0, 1\}^n \rightarrow \{0, 1\}$. Similar to the one-way communication application, when using shadow tomography to predict the outcome of a quantum copy-protected software, there is a gap in the accept probability. This promised gap in accept probability can reduce the sample complexity. In [1], Scott Aaronson introduced what we refer to as gapped shadow tomography, i.e. shadow tomography with the promise that the accept probabilities are gapped. He proved that gapped shadow tomography can be done using only $O(\log(m/\delta)/\epsilon^2)$ copies instead of the $O(\log(m^2)/\epsilon^4)$ of shadow tomography:

Proposition 1.6 (Sample upper bound of Gapped shadow tomography, Proposition 20 from [1]). *Given an unknown mixed state ρ and known two-outcome measurements M_1, \dots, M_m , along with real values $\epsilon, c_1, \dots, c_m \in [0, 1]$, assume that for each $i \in [m]$, we are promised that either $\text{Tr}[M_i\rho] \geq c_i$ or $\text{Tr}[M_i\rho] \leq c_i - \epsilon$. In this case, we can determine which condition holds for each $i \in [m]$ using $k = O(\log(m/\delta)/\epsilon^2)$ copies of ρ , with a success probability of at least $1 - \delta$.*

Note that the sample complexity of gapped shadow tomography is same as its “classical version”, which we defined as follows:

Problem 1.7 (Classical Gapped Shadow Tomography Problem). *Given an unknown diagonal density matrix ρ a set with diagonal measurements, M_1, \dots, M_m , and real values $\epsilon, c_1, \dots, c_m \in [0, 1]$, our goal is to discern if $\text{Tr}[M_i\rho] > c_i$ or $\text{Tr}[M_i\rho] < c_i - \epsilon$ for each $i \in \{1, \dots, m\}$. After implementing one measurement M_i on a copy, we obtain the outcome o_i .*

In Appendix A, we prove that the sample complexity of Problem 1.7 is $\Omega(\log(m/\delta))$, which matches the sample complexity of its quantum version, Proposition 1.6. Since the classical version is easier than the quantum version, both versions has sample complexity $\Theta(\log(m/\delta))$. Accordingly, having non-commuting measurements does not increase the sample complexity of gapped shadow tomography.

In our self-defined problem– Quantum Event Identification (QEI), we propose to predict $\text{Tr}[M_i\rho]$ for each measurement M_i with a success probability of $1 - \Delta$, rather than aiming to predict all measurements correctly with probability $1 - \delta$. The motivation behind this adjustment stems from the fact that in the classical version of the gapped shadow tomography problem, such a change allows us to achieve a sample complexity of $O(1)$, as explained in the follows. As stated in Lemma A.2, we can successfully predict each measurement with probability $1 - \Delta$ with $\Theta(\log(1/\Delta))$ copies. Moreover, since this is a classical problem, “measurements” for all m two-outcome measurements can be performed on a single sample simultaneously. If we choose Δ as a constant, the sample complexity is $O(1)$.

Since the quantum version of gapped shadow tomography is no harder than the classical version, we aim to explore the possibility that QEI also has the same sample complexity of its classical counterpart and can be done in $O(1)$ samples.

To investigate possibility that QEI could be achieved with $O(1)$ copies, we commence experimental simulations. Inspired by [2], where the Event Finding Problem 1.4 is addressed using only one copy, we develop a series of procedures to tackle the quantum event identification problem and use simulation tools to experimentally validate the feasibility of our approach.

In our simulation study, we first validate the performance of blended and random measurement methods proposed by [2] on the quantum event finding problem. Building on these validated methods, we derive multiple procedures for QEI and run simulations to assess their relative efficiency. Additionally, we implement the classical shadow method from [10] to evaluate whether it outperforms the derived procedures from [2]. Finally, we further analyze the performance of classical shadow procedure on QEI. Through these experiments, we provide a comprehensive assessment of our procedures’ efficiency in addressing Quantum Event Identification.

1.2 Outline

This thesis is organized as follows. In Chapter 2, we establish the foundational concepts and introduce the primary notation for quantum measurements and Event Learning Problem. This chapter lays the groundwork for understanding the core algorithms and procedures developed later.

In Chapter 3, we delve into the various procedures tailored for QEI and also introduce our measurement generating procedure. These include adaptations of existing methods such as blended and random measurements, as well as new techniques like the interweaving and three-outcome blended measurements. We also propose an optimization strategy for enhancing blended measurements and discuss how classical shadow is employed to handle QEI. Each procedure is explained in detail, along with its rationale and intended improvements over prior approaches.

Chapter 4 focuses on the simulation design and analysis. We describe the setup used to simulate quantum event learning, including parameters such as measurement dimensions, rank, and probability thresholds. The results of these simulations are presented through detailed comparisons of the procedures, showing their relative effectiveness in solving the quantum event identification problem. Special attention is given to the efficiency of each method, the influence of key variables such as the number of measurements and copies, and the behavior of classical shadow procedure in different test cases. The chapter also explores the impact of measurement constraints on the simulation outcomes.

2 Preliminary

In this thesis, we adopt the notation aligned with our primary reference [2]. A quantum measurement, specifically a positive-operator valued measure (POVM), is represented by a set $\{M_1, M_2, \dots, M_k\}$, where each M_i is an observable matrix in $\mathbb{C}^{d \times d}$, satisfying $0 \leq M_i \leq I$ and the completeness relation $\sum_i M_i = I$. The operators' square roots, $\{\sqrt{M_1}, \sqrt{M_2}, \dots, \sqrt{M_k}\}$, are termed "measurement operators" and serve as fundamental elements within quantum measurement frameworks.

In subsequent chapters, we will refer to "two-outcome measurements," represented by pairs $\{\sqrt{M}, \sqrt{I - M}\}$. A "set of two-outcome measurements" consists of collections with outcomes labeled as "accept" or "reject." We denote this set by \mathcal{M} , expressed as

$$\mathcal{M} = \{\{\sqrt{M_1}, \sqrt{I - M_1}\}, \dots, \{\sqrt{M_m}, \sqrt{I - M_m}\}\}.$$

For brevity, we may also write this ensemble as $\mathcal{M} = \{M_1, \dots, M_m\}$.

The acceptance probability for a measurement is given by $\text{Tr}[M_i \rho]$, where ρ represents the quantum state under observation. An outcome i indicates the acceptance of measurement M_i . In our simulations, we evaluate the success probability of each procedure by calculating the ratio of correctly matched outcomes, distinguishing between measurements with high and low acceptance probabilities.

Blended measurement 2.1 is proposed in [2] to solve the event learning problem. A blended measurement merges all rejected outcomes into one outcome; thus, we only know the outcome when it accepts, but we cannot determine which rejecting outcome is.

Definition 2.1 (Blended Measurement, [2]). *Given a set of two-outcome measurements $\mathcal{M} = \{M_1, M_2, \dots, M_m\}$, the blended measurement $\mathcal{E}(\mathcal{M})$ is defined to be the $(m + 1)$ -outcome measurement with measurement operators*

$$E_0 = \sqrt{1 - \sum_{i=1}^m \frac{M_i}{m}},$$

$$E_i = \sqrt{\frac{M_i}{m}}, \quad \text{for } i \in \{1, \dots, m\}.$$

We refer to outcome E_0 as the "reject" outcome, and outcomes E_1, \dots, E_m as the "accepting" outcomes.

Further, the two procedures proposed by the authors in [2] to address the event-finding problem 1.4 each rely on the repeated application of blended measurements and random measurements.

Procedure 1: Blended Measurement Procedure [2]

Blended Measurement Procedure

Input: A classical description of a set of two-outcome measurements $M = \{M_1, M_2, \dots, M_m\}$ and a single copy of a state ρ .

Output: ACCEPT or REJECT.

1. Prepare the quantum system in state ρ .
2. Repeat m times:
 - (a) Perform the blended measurement $\{M\}$ on the state. If the measurement accepts, return ACCEPT.
3. Return REJECT.

Procedure 2: Random Measurement Procedure [2]

Random Measurement Procedure

Input: A black-box implementation of each measurement in $M = \{M_1, M_2, \dots, M_m\}$ and a single copy of state ρ .

Output: ACCEPT or REJECT.

1. Prepare the quantum system in state ρ .
2. Repeat m times:
 - (a) Pick a random measurement $M_i \in M$.
 - (b) Perform the measurement M_i on the current state. If the measurement accepts, return ACCEPT.
3. Return REJECT.

In [2], the authors provide two bounds on the efficiency of using each procedure to solve the Event Finding Problem 1.4:

Theorem 2.2 (Blended Measurements on Event Finding, Theorem 31 from [2]). *Let $M = \{M_1, M_2, \dots, M_m\}$ be a set of two-outcome measurements. Let ρ be a state such that either: there exists an $i \in [m]$ with $\text{Tr}[M_i\rho] > 1 - \epsilon$ (Case 1), or $\sum_i \text{Tr}[M_i\rho] \leq \delta$ (Case 2). Also, define:*

$$\beta = \sum_{i: \text{Tr}[M_i\rho] < 1 - \epsilon} \text{Tr}[M_i\rho].$$

Then, if the blended measurement $B(M)$ is applied m times in sequence to a quantum system initially in state ρ : in Case 1, with probability at least

$$\frac{(1 - \epsilon)^3}{12(1 + \beta)},$$

at least one accepting outcome is observed, and the first accepting outcome observed corresponds to a measurement M_i with $\text{Tr}[M_i\rho] > 1 - \epsilon$. In Case 2, an accepting outcome is observed with probability at most δ .

Theorem 2.3 (Random Measurements on Event Finding, Theorem 32 from [2]). *Let $M = \{M_1, M_2, \dots, M_m\}$ be a set of two-outcome projective measurements, and define ρ , β , ϵ , and δ as above. Then, if measurements are chosen at random (with replacement) from M and applied to a quantum system initially in state ρ : in Case 1, with probability at least*

$$\frac{(1 - \epsilon)^7}{1296(1 + \beta)^3},$$

at least one measurement accepts, and the first accepting measurement is a measurement $M_i \in M$ with $\text{Tr}[M_i\rho] > 1 - \epsilon$. In Case 2, a measurement accepts with probability at most 2δ .

3 Method

In this chapter, we seek to demonstrate the efficiency of various procedures for the QEI problem. Our aim is to ensure that with these procedures, a constant success probability is achievable in QEI. This, in turn, ensures only constant sample complexity for the copies required.

Problem 3.1 (Quantum Event Identification). *Given an unknown mixed state ρ and known two-outcome measurements M_1, \dots, M_m , assume that for each $i \in [m]$, we are promised that either $\text{Tr}(M_i\rho) \geq c_i$ or $\text{Tr}(M_i\rho) \leq c_i - \epsilon$. We want to determine which of these conditions holds for each $i \in [m]$ so that, for every i , we successfully predict either $\text{Tr}[M_i\rho] \leq c_i - \epsilon$ or $\text{Tr}[M_i\rho] \geq c_i$ with a probability at least $1 - \Delta$. Note that the success probability $1 - \Delta$ is the success probability for predicting a single $\text{Tr}[M_i\rho]$.*

3.1 Measurements Generating

Before implementing the procedures, it is necessary to generate a testing set. Without loss of generality, we pick the "unknown state" as $|0\rangle$, and generates measurements satisfying the required conditions. These conditions include the acceptance probability $\text{Tr}[M_i\rho]$, as well as the rank, dimension of M_i . Ideally, the generated measurement set should be as close to the theoretically worst-case scenario as possible. However, obtaining the worst case is theoretically challenging and beyond the scope of this research. Instead, we utilize the Haar random case to ensure that the measurement set remains sufficiently challenging.

The acceptance probability of a random measurement that satisfies the requirement often falls into extremes—it is either fairly high or fairly low ($\text{Tr}[M_i\rho] \leq c_i - \epsilon$ or $\text{Tr}[M_i\rho] \geq c_i$). For our test we set $c = 0.9$ and $\epsilon = 0.8$. Due to hardware constraints, directly sampling measurements that meet the acceptance probability threshold by simply rotating the projector for every sample is impractical. To address this, we propose a computationally efficient procedure for generating a measurement set satisfying the requirement.

Let the projector $P = \text{diag}(\underbrace{0, 0, \dots, 0}_{d-r \text{ zeros}}, \underbrace{1, 1, \dots, 1}_{r \text{ ones}})$, which is a $d \times d$ matrix with rank r . The simplest method to generate a measurement M_i with Haar-random involves creating a random unitary U and rotating P as $M_i = U^\dagger P U$. However, this approach is computationally expensive in relatively high dimension, as it requires substantial time and resources to filter and identify M_i that satisfy the desired acceptance probability. To improve efficiency while preserving Haar-random, we instead use the following process to find a suitable U with a special vector V :

1. **Sampling the accept probability p :** We first sample a probability p that satisfies the acceptance probability threshold ($p \geq c_i$ or $p \leq c_i - \epsilon$) while maintaining Haar-random properties. This is

achieved by truncating the normal distribution within specified ranges, such as $0 \sim c_i - \epsilon$ or $c_i \sim 1$, to ensure that the sampled p adheres to the constraints and is sufficiently random.

2. **Generating the Special Vector V :** Next, we construct a vector V of the form:

$$V = \begin{bmatrix} a_1 & \dots & a_{d-r} & b_1 & \dots & b_r \end{bmatrix}$$

where $\{a_i\}$ and $\{b_i\}$ are Haar-randomly generated complex vectors with their norm satisfy the conditions:

$$\sum_{i=1}^{d-r} |a_i|^2 = 1 - p \quad \text{and} \quad \sum_{i=1}^r |b_i|^2 = p.$$

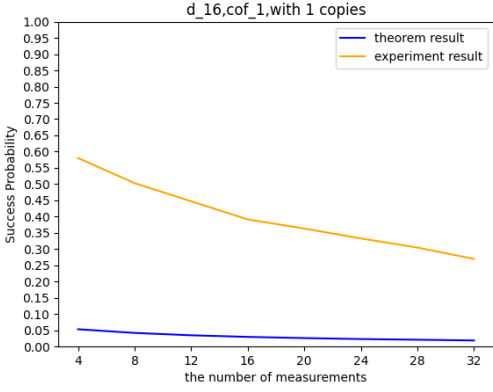
Constructing V this way ensures that the measurement's acceptance probability will match the sampled p later in the process.

3. **Constructing the Unitary U_r :** To construct the unitary matrix U_r , we begin by replacing the first column of a Haar-randomly generated unitary matrix U with the vector V . Next, we perform a QR decomposition on U . The resulting orthogonal matrix Q from the QR decomposition serves as the desired unitary U_r , ensuring that its first column remains V . This guarantees that the acceptance probability aligns with the sampled p .
4. **Rotating the Projector:** Using U_r , we generate the measurement M_i as:

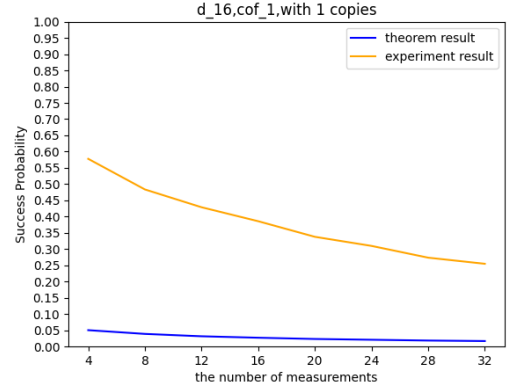
$$M_i = U_r^\dagger P U_r.$$

This guarantees that $\text{Tr}[M_i \rho] = p$, where p is the probability sampled in the first step.

This procedure significantly accelerates the measurement generation process while preserving sufficient randomness in M_i . To validate the correctness of our approach, we conducted a simulation demonstrating that the measurement generation procedure using the special vector effectively approximates Haar-randomness. In Figure 1, we compare the success probabilities for solving the event-finding problem with blended measurement in Case 1 using measurements generated by the special vector procedure and those generated by Haar-randomly selected unitaries to rotate the projector. The results show that the procedure utilizing the special vector achieves a success probability nearly identical to that of the Haar-random approach. For computational feasibility, the simulation dimension was reduced to 16, compared to the standard dimension of 64 used in our other simulations.



(a) The Measurement Generating Procedure with Special Vector



(b) The Measurement Generating Procedure with Haar-Randomly Selected Unitaries

Figure 1: Comparison of the Success Probability in Event Finding Case 1 with Different Measurement Generating Procedures

3.2 Procedures

We developed six procedures specifically tailored for the QEI problem. Initially, we extended Procedure 1 and Procedure 2 to generate additional outputs to accommodate QEI, which features a number of high accepting probability outcomes (Procedure 3.2.1 and Procedure 3.2.2). Next, by modifying the structure of blended measurements, we introduced three novel procedures: "Interweave" (Procedure 3.2.3) combines the standard blended measurement set with its inverse, "Blended Three" (Procedure 3.2.4) minimizes blended measurement outcomes while maximizing the number of measurements per outcome, using majority voting for outcome selection and "Optimizing Blended" (Procedure 3.2.5) seeks to enhance the acceptance probabilities across all operators in the measurement set. Lastly, we (Procedure 3.2.6) leverages the classical shadow technique to tackle QEI.

The preliminary step for these procedures involves generating a set of two-outcome measurements, based on parameters d (dimension), r (rank), m (number of measurements), and s (portion of high acceptance measurements, set to $m/2$). Initially, half of the measurements satisfy $\text{Tr}[M_i\rho] > c_i$, indicating high acceptance probabilities, while the other half satisfy $\text{Tr}[M_i\rho] < c_i - \epsilon$, indicating low acceptance probabilities. To increase flexibility, we introduce a parameter α , which adjusts the number of repetitions for each measurement on the state ρ .

3.2.1 Procedure 3: Special Blended measurement for QEI

Special Blended measurement for QEI

Input: A black-box implementation of each measurement in $M = \{M_1, M_2, \dots, M_m\}$, c copies of state ρ .

Output: $O = \{o_1, \dots, o_{m/2}\}$, $1 \leq o_i \leq m$, where each o_i is the index of a measurement with high accepting probability.

1. Generate the blended measurement set \mathcal{E} as defined in Definition 2.1.
2. Initialize a counting table $\mathcal{T} = \{t_1, \dots, t_m\}$, with each $t_i = 0$.
3. Repeat the following process c times:
 - (a) Initialize a quantum system in the state ρ .
 - (b) Execute $\alpha \times m$ iterations, with each iteration involving:
 - i. Perform a measurement using the blended measurement set \mathcal{E} on ρ . If the measurement M_i accepts, increment t_i by 1.
4. From the counting table \mathcal{T} , identify the indices corresponding to the top half with the highest frequency of acceptance as the outcome set O . If the number of unique outcomes is less than $m/2$, randomly select additional indices from the less frequent outcomes to complete the set.

3.2.2 Procedure 4: Special Random measurement for QEI

Special Random measurement for QEI

Input: A black-box implementation of each measurement in $M = \{M_1, M_2, \dots, M_m\}$, a single copy of state ρ .

Output: $O = \{o_1, \dots, o_{m/2}\}$, $1 \leq o_i \leq m$, where each o_i is the index of a measurement with high accepting probability.

1. Initialize a counting table $\mathcal{T} = \{t_1, \dots, t_m\}$, with each $t_i = 0$.
2. Repeat the following process c times:
 - (a) Prepare a quantum system in the state ρ .
 - (b) Shuffle the measurements in the set M .
 - (c) Execute m iterations, with each iteration involving:
 - i. Select the next measurement M_i from the shuffled set M , ensuring no repetition.
 - ii. Perform the measurement M_i on the state ρ . If the measurement M_i accepts, increment t_i by 1.
3. From the counting table \mathcal{T} , identify the indices corresponding to the top half with the highest frequency of acceptance as the outcome set O . If the number of unique outcomes is less than $m/2$, randomly select additional indices from the less frequent outcomes to complete the set.

3.2.3 Procedure 5: Interweaving Blended measurement for QEI

The Interweaving Blended Measurement procedure utilizes inverse blended measurements 3.2, which are specifically designed to identify outcomes with low acceptance probabilities. This approach strategically amplifies the distinction between the set of measurements yielding high acceptance probabilities and those with low acceptance probabilities. The inverse blended measurement blends the accepting outcome while keeping the rejecting outcomes unchanged. In other words, we cannot distinguish which measurement was accepted, but we do know which one was rejected.

Definition 3.2 (Inverse Blended Measurement). *Given a set of two outcome measurements $\mathcal{M} = \{M_1, M_2, \dots, M_m\}$ the inverse blended measurement \mathcal{E}_{inv} is defined to be the $m+1$ outcome measurement with measurement operators*

$$E_0 = \sqrt{1 - \sum_{i=1}^m \frac{1 - M_i}{m}}$$

$$E_i = \sqrt{\frac{1 - M_i}{m}} \text{ for } i \in \{1, \dots, m\}$$

We refer to outcome E_0 as the "accept" outcome, and outcomes E_1, \dots, E_m as "rejecting outcomes."

Interweaving Blended measurement for QEI

Input: A black-box implementation of each measurement in $M = \{M_1, M_2, \dots, M_m\}$, and c copies of state ρ .

Output: $O = \{o_1, \dots, o_{m/2}\}$, $1 \leq o_i \leq m$, where each o_i is the index of a measurement with high accepting probability.

1. Generate the blended measurement set \mathcal{E} according to 2.1, and the inverse blended measurement set \mathcal{E}_{inv} according to 3.2.
2. Initialize a counting table $T = \{t_1, \dots, t_m\}$, with each $t_i = 0$.
3. Repeat the following process c times:
 - (a) Initialize a quantum system in the state ρ .
 - (b) Execute $(\alpha \times m)/2$ iterations, with each iteration involving:
 - i. Perform a measurement using the inverse blended measurement set \mathcal{E}_{inv} on ρ . If the measurement M_i accepts, decrement t_i by 1.
 - ii. Perform a measurement using the measurement set \mathcal{E} on ρ . If the measurement M_i accepts, increment t_i by 1.
4. From the counting table T , identify the indices corresponding to the top half with the highest frequency of acceptance to form the outcome set O . If the number of unique outcomes is less than $m/2$, randomly select additional indices from the less frequent outcomes to complete the set.

3.2.4 Procedure 6: Three-outcome Blended measurement for QEI

In the three-outcome blended measurement procedure, we introduce another measurement process, defined as a three-outcome blended measurement 3.3. This procedure modifies the original blended measurement to limit the number of outcomes to three. Apart from the reject outcome, the other two outcomes are derived by aggregating each half of the two-outcome measurement set. The rejecting outcome includes all reject outcomes from all measurements, while the other two accept outcomes blend the accept outcomes from the top and bottom halves of the measurements, respectively.

Definition 3.3 (Three-outcome Blended Measurement). *Given a set of two outcome measurements $\mathcal{M} = \{M_1, M_2, \dots, M_m\}$ three-outcome blended measurement \mathcal{E}_{three} is defined to be the three outcome measurement with measurement operators*

$$E_0 = \sqrt{1 - \sum_{i=1}^m \frac{M_i}{m}}$$

$$E_1 = \sqrt{\frac{\sum_{i=1}^{m/2} M_i}{m}}$$

$$E_2 = \sqrt{\frac{\sum_{i=(m/2)+1}^m M_i}{m}}$$

We refer to outcome E_0 as the "reject" outcome, and outcomes E_1, E_2 as "accepting outcomes."

Three-outcome Blended measurement for QEI

Input: A black-box implementation of each measurement in $M = \{M_1, M_2, \dots, M_m\}$, and c copies of state ρ .

Output: $O = \{o_1, \dots, o_{m/2}\}$, $1 \leq o_i \leq m$, where each o_i is the index of a measurement with high accepting probability.

1. Initialize a counting table $T = \{t_1, \dots, t_m\}$, with each $t_i = 0$.
2. Repeat the following process c times:
 - (a) Initialize a quantum system in the state ρ .
 - (b) Execute $5 \times m$ iterations, with each iteration involving:
 - i. Shuffle the measurements in M .
 - ii. Generate the three-outcome measurement \mathcal{E}_{three} according to Definition 3.3.
 - iii. Perform the measurement \mathcal{E}_{three} on ρ . If the measurement E_1 or E_2 accepts, increment the counts t_j, \dots, t_k for the corresponding measurements M_j, \dots, M_k that are part of the accepted E_i by 1.
3. From the counting table T , identify the indices corresponding to the top half with the highest frequency of acceptance to form the outcome set O . If the number of unique outcomes is less than $m/2$, randomly select additional indices from the less frequent outcomes to complete the set.

3.2.5 Procedure 7: Optimizing Blended measurement for QEI

In the optimizing blended measurement procedure, we aim to amplify each acceptance probability, regardless of whether it is high or low. To achieve this objective, we introduce Optimizing Blended Measurement 3.4, which uses the optimizing factor– f to achieve the amplification of the accepting probability.

Definition 3.4 (Optimizing Blended Measurement). *Given a set of two outcome measurements $\mathcal{M} = \{M_1, M_2, \dots, M_m\}$, we can compute the optimizing factor q ,*

$$S = \sum_{i=1}^m M_i$$

$$q = \frac{1}{(\lambda_{max}/m)}$$

we can get the λ_{max} from the S , and normalize it by dividing m . Afterward, we obtain q . The optimizing blended measurement \mathcal{E}_{opt} is defined to be the $m+1$ outcome measurement with measurement operators:

$$E_0 = \sqrt{1 - q \sum_{i=1}^m \frac{1 - M_i}{m}}$$

$$E_i = \sqrt{q \frac{1 - M_i}{m}} \text{ for } i \in \{1, \dots, m\}$$

We refer to outcome E_0 as the "accept" outcome, and outcomes E_1, \dots, E_m as "rejecting outcomes."

Optimizing Blended measurement for QEI

Input: A black-box implementation of each measurement in $M = \{M_1, M_2, \dots, M_m\}$ and c copies of state ρ .

Output: $O = \{o_1, \dots, o_{m/2}\}$, $1 \leq o_i \leq m$, where each o_i is the index of a measurement with high accepting probability.

1. Initialize a counting table $T = \{t_1, \dots, t_m\}$, with each $t_i = 0$.
2. Generate the measurement set \mathcal{E}_{opt} according to Definition 3.4.
3. Repeat the following process c times:
 - (a) Initialize a quantum system in the state ρ .
 - (b) Execute $\alpha \times m$ iterations, with each iteration involving:
 - i. Perform a measurement using the measurement set \mathcal{E}_{opt} on ρ . If the measurement M_i accepts, increment t_i by 1.
4. From the counting table T , identify the indices corresponding to the top half with the highest frequency of acceptance to form the outcome set O . If the number of unique outcomes is less than $m/2$, randomly select additional indices from the less frequent outcomes to complete the set.

3.2.6 Procedure 8: Classical Shadow for QEI

The most distinctive procedure is the Classical Shadow procedure for quantum event identification problem. By adapting the original Classical Shadow [10], we utilize the predicted state to compute the acceptance probability of the two-outcome measurement set. This allows us to make predictions about which measurements are most likely to have high acceptance probabilities.

Classical Shadow for QEI

Input: $M = \{M_1, M_2, \dots, M_m\}$, and c copies of the quantum state ρ .

Output: An array $O = \{o_1, o_2, \dots, o_{m/2}\}$, where each o_i is the index of a measurement with high accepting probability.

1. For each copy from 1 to c :
 - (a) Apply a random unitary U from a fixed ensemble to the state ρ .
 - (b) Perform a computational basis measurement to obtain an outcome b .
 - (c) Store the result and the selected unitary U in classical memory.
 - (d) Compute a classical snapshot using the inverse channel \mathcal{M}^{-1} , defined as $\mathcal{M}^{-1}(U^{-1}\text{diag}(b)U)$, where U^{-1} is the inverse of the unitary applied to the classical description of the outcome b .
2. Aggregate all classical snapshots $\hat{\rho}_i$ to form the classical shadow $S(\rho; c)$.
3. For each measurement from M_1 to M_m :
 - (a) Compute the trace $\text{Tr}[M_i \hat{\rho}_i]$ for each snapshot in $S(\rho; c)$.
 - (b) Calculate the median of $\text{Tr}[M_i \hat{\rho}_i]$ across all snapshots, denoting this as the predicted probability p_i .
4. Select the top half of measurements based on their median probabilities p_i to form the output set O .

4 Result

In this section, we present plots derived from the simulation results and analyze the insights gained. The coefficients for each test case vary across methods, ranks, and other factors, yielding insights regarding the mechanisms of event identification.

4.1 Simulation Premise

We begin by introducing the tools that support our simulation. Qiskit, the primary framework for constructing the simulation circuits, is an open-source quantum computing software development platform. It provides extensive tools for creating and managing quantum programs and facilitates execution on simulators and actual quantum hardware. Our project is developed using Python 3.10.12, with data analysis and visualization performed using packages like 'matplotlib' and 'pandas'. A key aspect of our simulation is the construction of the measurement set for the event learning problem. While detailed code is omitted here, we provide a summary of the process for constructing these measurement sets. Full implementation is available on our GitHub repository.

For various problems, we employ two types of measurement sets. For the event-finding problem, the set includes only one high-acceptance-probability outcome. In contrast, for quantum event identification, half of the outcomes have high acceptance probabilities. Apart from the high-probability outcomes, both sets share common attributes such as dimension, rank, number of measurements, and thresholds for high and low probabilities:

- Dimension (d) : the dimension of the measurement
- The Number of Measurements (m): the number of measurements in one two-outcome measurement set
- Rank (r) : the rank of the measurement
- High Probability (h_pro) : threshold for high acceptance probability, where measurements satisfy $Tr[M_i\rho] > h_pro$
- Low Probability (l_pro) : threshold for low acceptance probability, where measurements satisfy $Tr[M_i\rho] < l_pro$

These parameters enable us to construct varied measurement sets and analyze their impact on test outcomes. Due to hardware limitations, the dimension (d) is fixed at 32 for QEI and at 64 for the quantum event finding experiments. The number of measurements (m) ranges from 4 to 24 for QEI, and from 4 to 32 for quantum event finding, enabling us to evaluate efficiency across various settings. For the rank, we select $r = d/2$, based on theoretical and experimental results of Section 4.2.3, The effect of constraints of the classical shadow, as it represents the worst case for our simulation.

In the quantum event finding simulations, we employ 50 distinct measurement sets, each run 100 times, and derive success and failure rates from these trials. For QEI, we utilize 10 different measurement sets, each tested 250 times. The success rate for each measurement M_i is computed over these 250 runs, and the overall success rate of each measurement set is defined as the minimal success rate achieved among all measurements M_i .

Beyond measurement adjustments, we enhance the flexibility and performance of our procedures by tuning the coefficients α and c :

- α : Multiplier for the number of implementations of each measurement.
- c : Number of copies used in each run of the procedure.

These parameters are essential for controlling the dynamics of the experimental process.

4.2 Simulation Result

After outlining the premise of our simulation setting, we are now prepared to present the results. These are divided into two main parts: ‘The Validity of the Bounds in the Event Finding Problem’, ‘The Efficiency of Each Procedure for the Quantum Event Identification Problem.’ Additionally, there is a sub-part, ‘The effect of constraints of the classical shadow’, to observe how $\|M_i\|_{\text{shadow}}^2$ effects the experimental result.

4.2.1 The Validity of the Bounds in the Event Finding Problem

We examine the validity of the bounds (Theorem 2.2 and Theorem 2.3) for the event finding problem, as proposed in [2]. In our simulation, the results are consistent with theoretical expectations. The bounds for both methods, blended and random, are valid for Case 1 and Case 2. However, the lower bounds for Case 1 are not tight for either method, and this issue is more significant for random measurements.

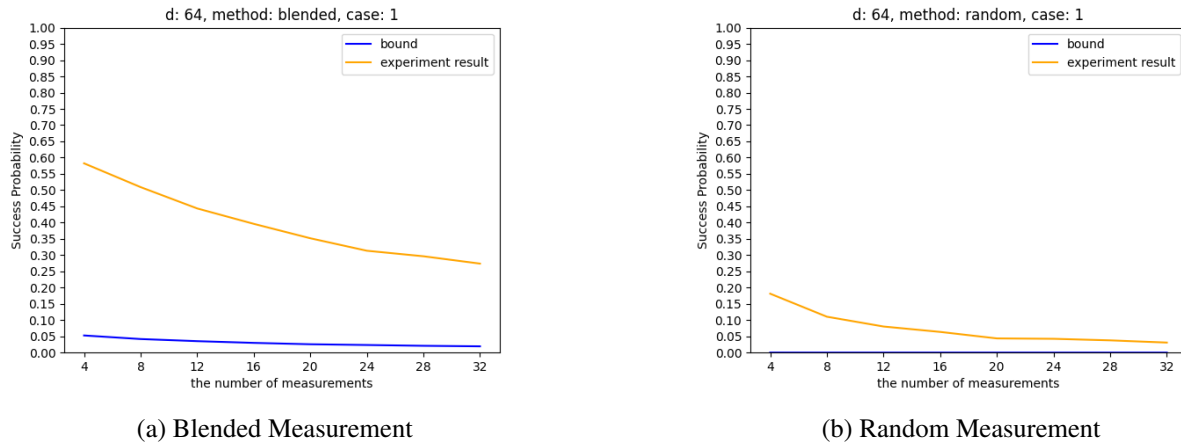


Figure 2: Comparison of Random and Blended Measurement in Case 1

In Figure 2, for the blended measurement, we observe that the experimental results and the lower bound follow similar trends, despite a noticeable gap between the two lines. In contrast, for the random measurement, the lower bound is positioned extremely close to the bottom of the figure. This is due to the significantly large constant in the theorem (involving division by 1296 in $(1 - \epsilon)^7 / (1296(1 + \beta)^3)$), rendering the lower bound for the random measurement barely visible. Nonetheless, both lower bounds remain valid, though not sufficiently tight. Moreover, we can extract more information from the figure 2. The success rate of the blended measurement is higher than that of the random measurement at every point, and its decline in success rate is more gradual, suggesting that it outperforms the random measurement in our test case.

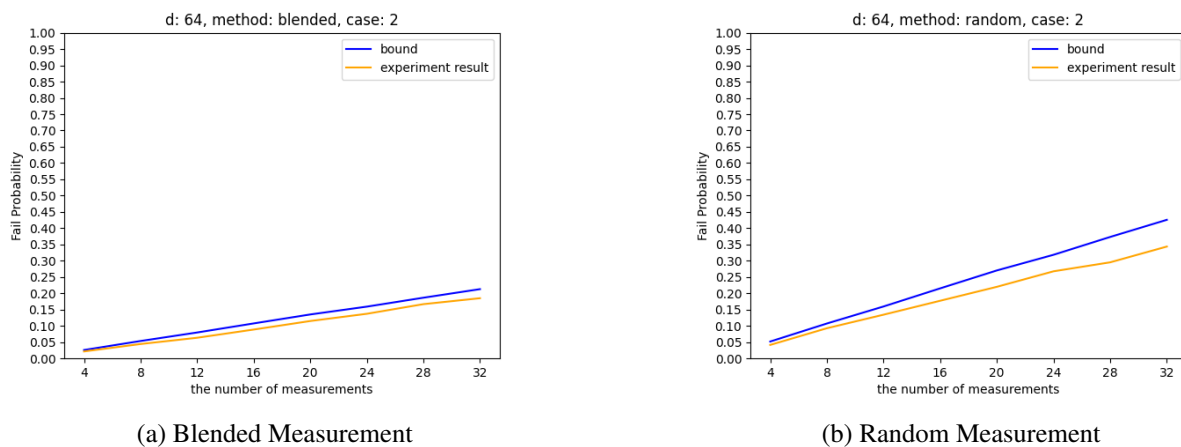


Figure 3: Comparison of Random and Blended Measurement in Case 2

In Figure 3, we compare the failure probabilities for the event finding problem in Case 2 using random and blended measurements. As the figure shows, for both methods, the experimental results closely align with the upper bound, indicating that the theoretical bound is sufficiently tight. Furthermore, the figure demonstrates that the failure probability of random measurement is consistently higher than that of blended measurement.

In our simulation case, the theoretical bounds in [2] are verified successfully. However, for the Case 1, we could expect the lower bounds could be improved in the future. Given the reliability of the theorems and procedures, we further utilize and adapt these two measurement methods for our self-defined problem, QEI.

4.2.2 The Efficiency of Each Procedure for the Quantum Event Identification Problem

In this section, we present the experimental results for Quantum Event Identification problem using different procedures. Specifically, the procedures are divided into three categories: the random measurement procedure, the derivative procedures from the blended measurement, and the Classical Shadow procedure. First, we conduct a comprehensive comparison of all procedures.

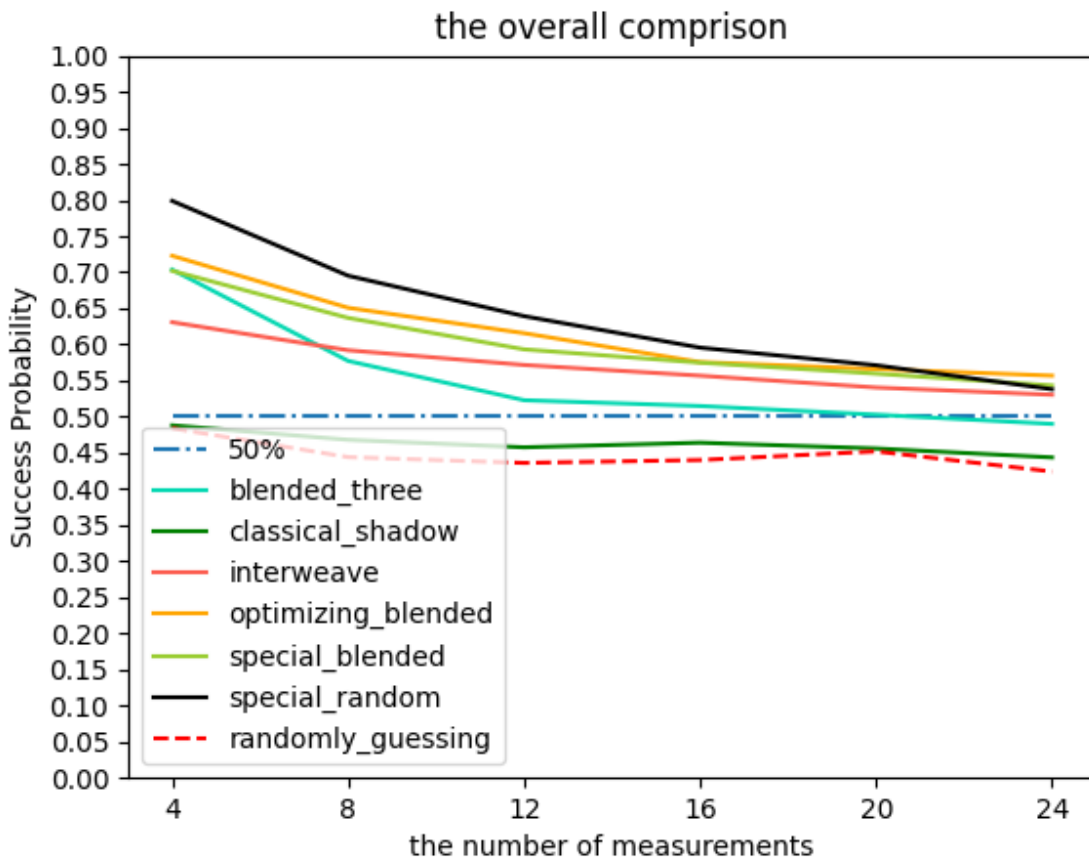


Figure 4: Overall Success Rate Comparison

The results depicted in Figure 4 visually illustrate how each procedure's success rate evolves as the number of measurements increases from 4 to 24. Except for the Classical Shadow procedure, all meth-

ods maintain success probabilities above the 50% reference line, demonstrating their relative effectiveness for the QEI task. The Classical Shadow procedure, in contrast, appears consistently below 50%, raising questions about its performance compared to simple guessing.

At first glance, this result may seem counterintuitive, as one would expect random guessing to average around 50% success per measurement. The key lies in our evaluation methodology: rather than averaging performance across all measurements, we focus on the single worst success rate within the entire measurement set. This “worst-case” assessment disproportionately penalizes the Classical Shadow procedure, pushing its observed success rate below the intuitive baseline of random guessing. Nevertheless, as indicated in the figure, the Classical Shadow curve still remains above the red dashed line that represents the worst possible scenario for random guessing. This observation confirms that while the Classical Shadow procedure is disadvantaged by our worst-case metric, it does not truly perform worse than an entirely random strategy.

Upon closer inspection, the different derivations of the blended measurement procedure exhibit nearly identical success rate trends, with the exception of the three-outcome blended procedure. As depicted in Figure 5, procedures derived from blended measurement demonstrate highly consistent trends, reflecting the inherent stability of these approaches across varying test cases.

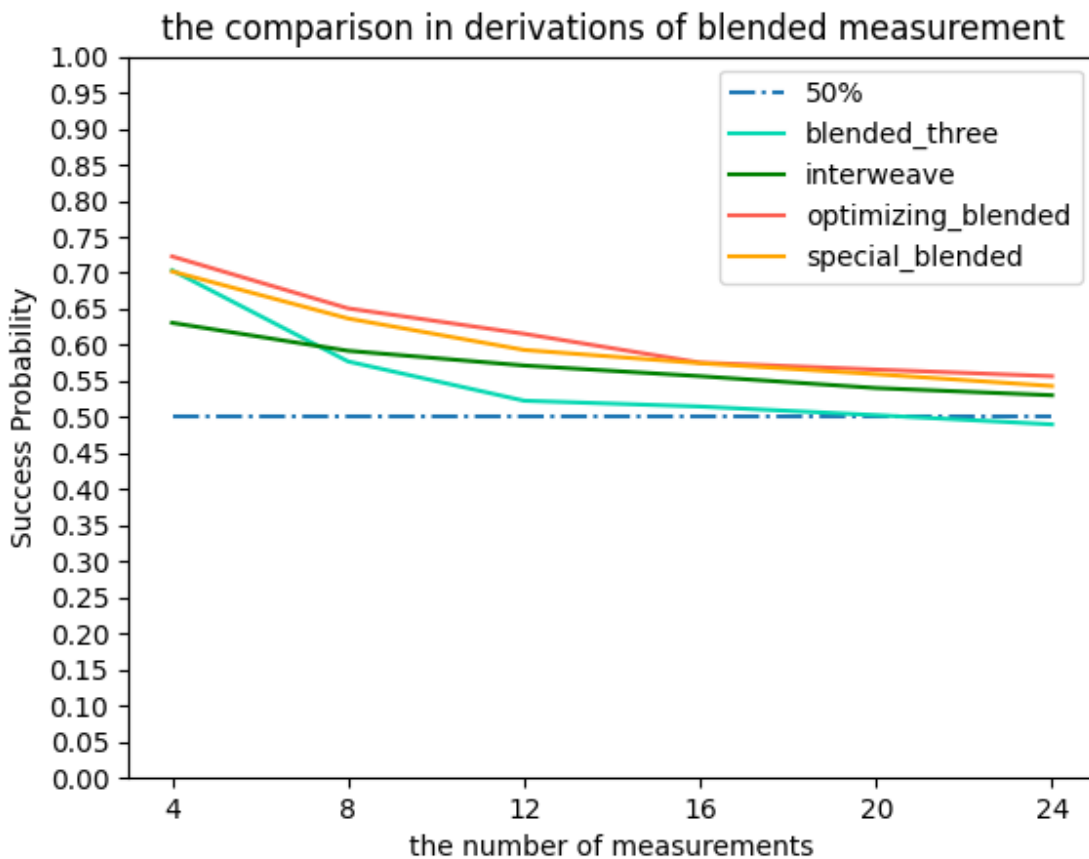


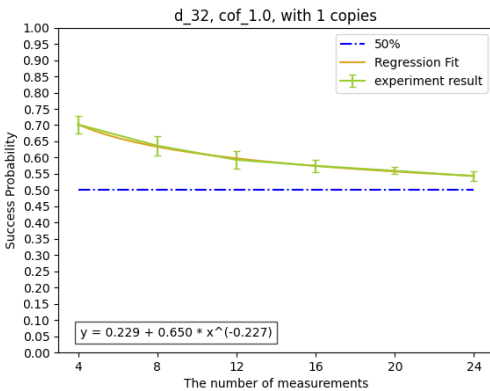
Figure 5: Comparison in Blended Measurement Derivations

Additional insights can be gleaned from Figure 6, which compares the blended and random measurement procedures. In random measurement procedure, the initial success rate at around four measurements

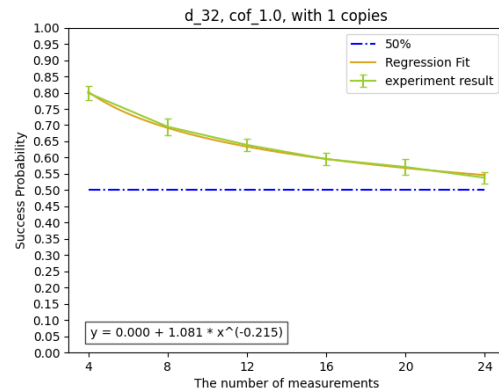
is notably higher—close to 0.8—indicating a strong initial advantage. However, as the number of measurements increases, the success rate decreases more rapidly, with the regression fit approaching a near-zero baseline. This suggests that while random measurements can yield high early success rates, its advantage erodes more steadily as additional measurements are introduced.

In contrast, blended measurement procedure begins at a somewhat lower initial success rate (approximately 0.7), but its regression model includes a positive baseline term (0.229). This implies that as the number of measurements grows, the success rate stabilizes at a level significantly above zero. Consequently, although the blended approach may not achieve the same high starting point as the random method, it offers a more resilient long-term performance.

Random measurement procedure excels in initial performance but loses its advantage as the number of measurements increases. In contrast, blended measurement procedure may not begin as strongly, yet it maintains a more favorable success rate as the system scales. This difference in long-term behavior suggests that the blended measurement procedure may be more robust in scenarios involving a larger number of measurements. It is also worth noting that, in most practical settings, the number of measurements does not exceed the dimension of the system, preventing the scenario from ever truly approaching an infinite regime or dropping below the baseline of random guessing.



(a) Regression of Blended Measurement Procedure



(b) Regression of Random Measurement Procedure

Figure 6: Regression and Comparison

Subsequently, we tried to adjust the factor α , mentioned in the premise of simulation, to see what might be changed in the result. α is from 0.6 to 2.2, applied on three procedures- special blended, optimizing blended, and interweave.

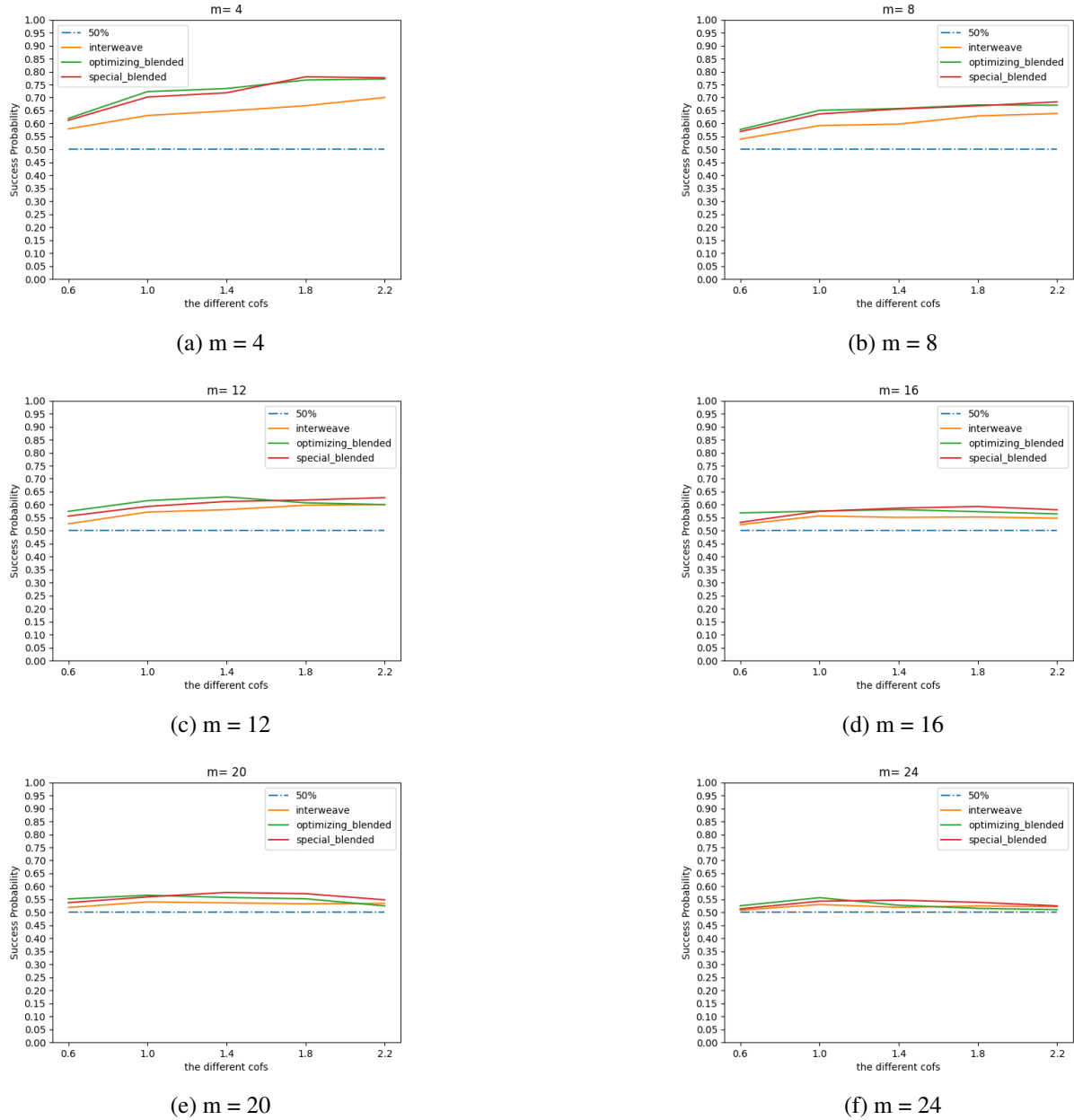
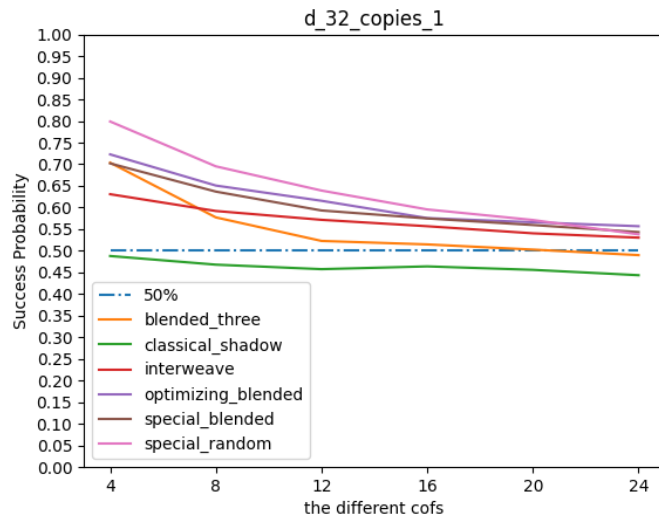


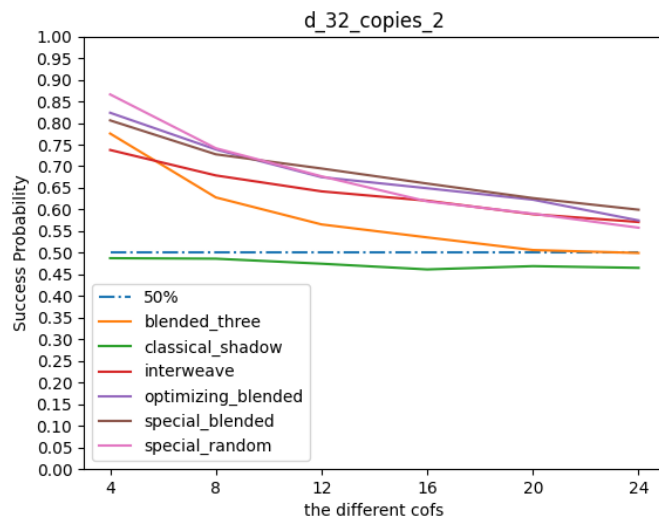
Figure 7: Comparison with Different α across All Numbers of Measurements

These six plots demonstrate that the effect of α diminishes as the number of measurements increases. Furthermore, the impact of α becomes negligible once α exceeds 1. This phenomenon is most evident in the plot where $m = 4$. Based on this result, we recommend setting α to 1 for any test case to achieve high efficiency in a shorter time.

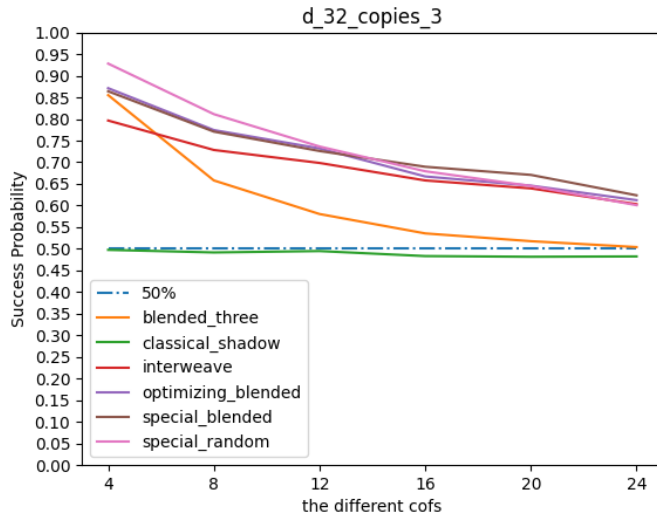
So far, we have presented the experimental results using only one copy. We also tested the case with multiple copies to examine how increasing the number of copies affects the success rate. In the multiple-copy tests, we used one to three copies for each approach, and the improvements were significant.



(a) The Success Rate with 1 Copy



(b) The Success Rate with 2 Copies



(c) The Success Rate with 3 Copies

Figure 8: Comparison with Different Numbers of Copies

In Figure 8, as the number of copies increases, the overall efficiency improves across all approaches. Although our primary objective is to achieve high efficiency using only one copy per test, we present the multi-copy cases to demonstrate the potential strength of these procedures. Furthermore, with up to three copies, we observe consistent trends in the efficiencies of the methods. Notably, the results from the special random procedure exhibit a sharper decline compared to those derived from blended measurements, and the gap between each result widens as the number of copies increases.

4.2.3 The effect of constraints of the classical shadow

Due to the low success rate of the classical shadow procedure over one to three copies, we aim to determine how many copies are needed for it to achieve a success rate similar to that of other methods. Also, we can have a better observation of the effect of $\|M_i\|_{\text{shadow}}^2$ with higher copies. Thus, we incrementally increased the number of copies until its performance approached the efficiency of the other approaches. As a result, the figure 9 implies that using at least 20 copies allows us achieving the similar probability with others'.

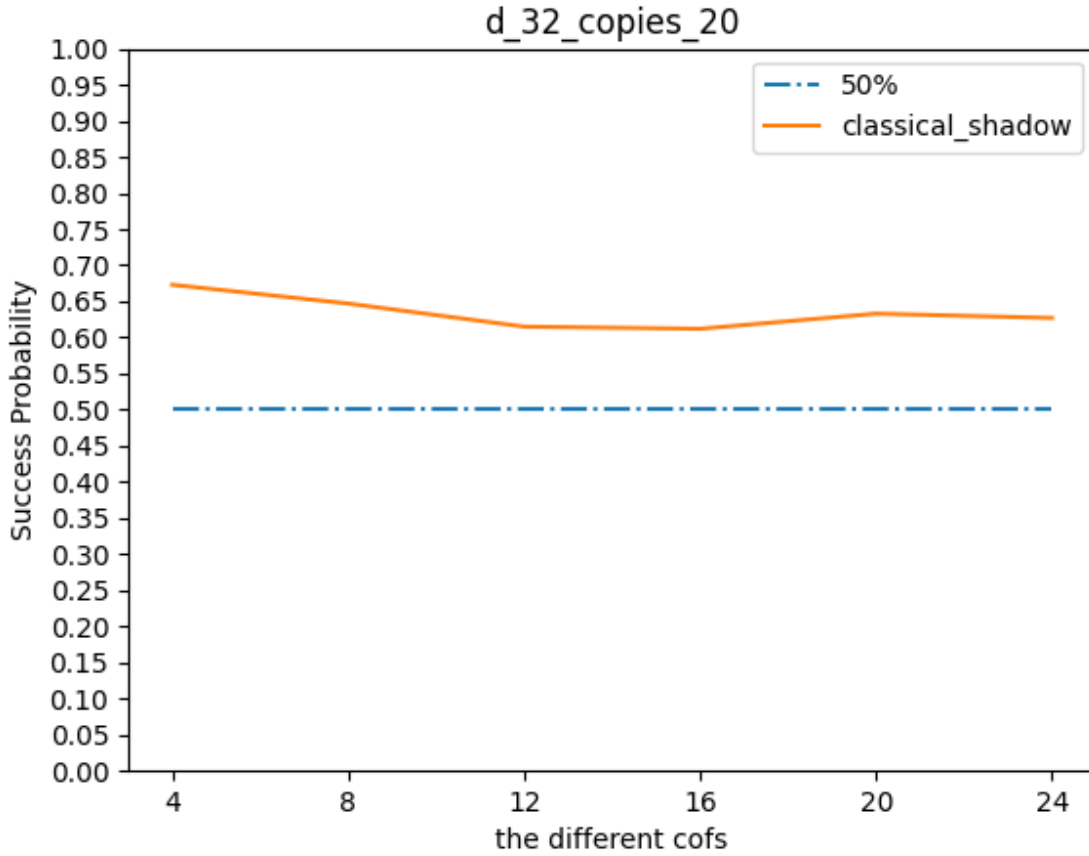


Figure 9: Classical Shadow Procedure with 20 Copies

Subsequently, considering the constraints of classical shadow tomography as mentioned in Chapter 1, we tested measurement sets of different ranks to observe whether the rank affects our results when using only one copy of the quantum state. In [10], the authors provide constraints for random Clifford measurements, noting that the shadow norm is closely related to $\text{Tr}(M_i^2)$, which can be approximately treated as the rank of the measurement. With ranks ranging from 4 to 28 and the number of measurements ranging from 8 to 16, we ran the classical shadow procedure on a quantum event identification problem using 20 copies of the state.

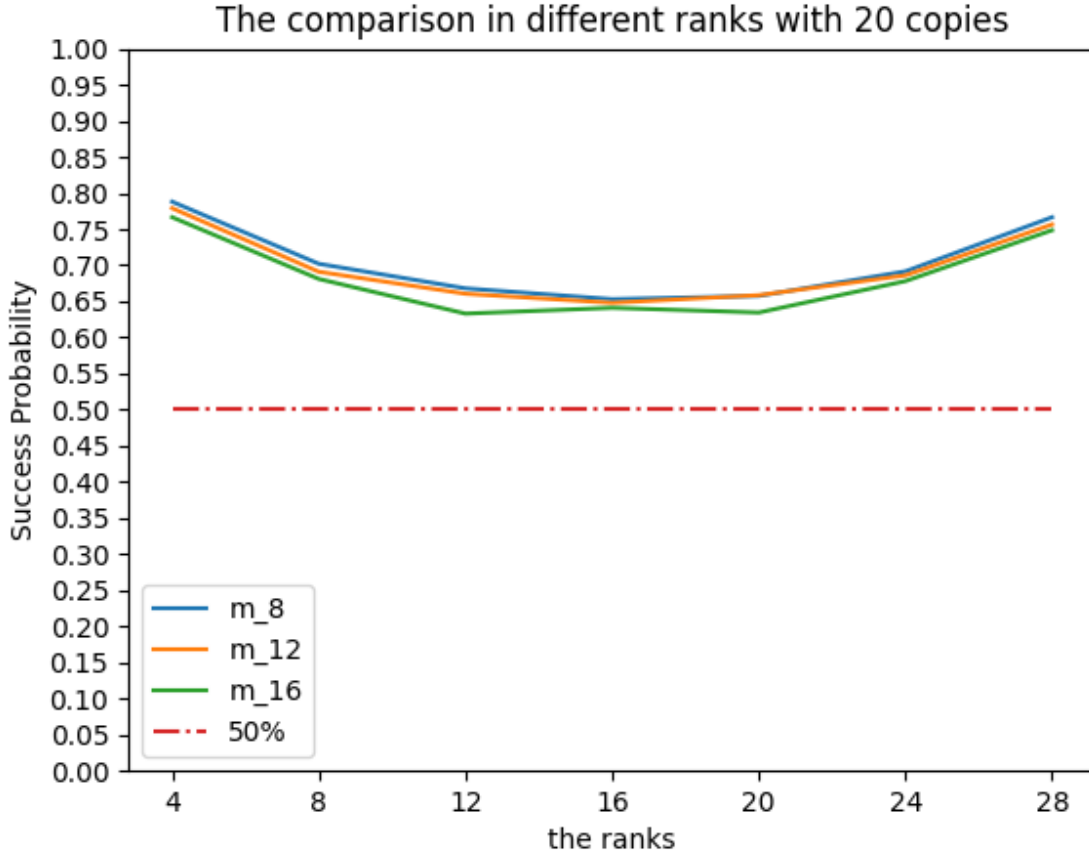


Figure 10: Classical Shadow Procedure’s Results with Different Ranks

As shown in Figure 10, the experimental results follow the trend outlined by the constraint $\|M_i\|_{\text{shadow}}^2$. Recalling the expression from the introduction:

$$N \geq O\left(\frac{\log m}{\epsilon^2} \max_i \|M_i\|_{\text{shadow}}^2\right),$$

this equation depicts that more copies are required for higher shadow norms (i.e., higher-rank measurements). In other words, lower-rank measurements should yield better results than higher-rank measurements when using the same number of copies. As seen in the figure, the plot is symmetric with respect to rank, which makes sense because ranks 4 and 28 are equivalent in significance for a dimension of 32. Therefore, the most challenging measurement set corresponds to rank $d/2$, or rank 16, which we selected as our general test measurements.

4.3 Discussion

In this work, we have simulated the Quantum Event Identification (QEI) problem using various measurement procedures, validated the efficiency bounds established in [2], and illustrated the influence of shadow norms described in [10].

Our simulations show that most procedures maintain a stable success rate of approximately 60% at $m = d/2$ (Figure 4), even when only a single copy is available in low-dimensional systems. By contrast, the classical shadow procedure requires about 20 copies to achieve similar performance levels (Figure 9). This result shows the potential of the blended measurement and random measurement to solve QEI.

Moreover, our results confirm the theoretical predictions for both blended and random measurement strategies presented in [2]. While these theoretical bounds provide a robust upper limit for the efficiency of case 2 in quantum event finding, they offer a relatively looser lower bound for case 1. Nevertheless, both sets of bounds hold true and remain applicable within our simulation environment.

Additionally, we highlight the critical role of shadow norms introduced in [10]. Our findings indicate that lower shadow norms—commonly associated with lower-rank measurements—lead to higher success probabilities in quantum event identification, as evidenced in Figure 10. This relationship validates the choice of measurement ranks in our QEI test setting.

In summary, our simulations reinforce the theoretical foundations of QEI, elucidate the significance of measurement design and sample complexity, and emphasize the central influence of shadow norms on success rates.

4.4 Conclusion

We introduced the Quantum Event Identification (QEI) problem as an approach to efficiently identify measurements with high success rates. By leveraging a promise gap and focusing on individual measurement predictions, QEI presents a promising framework that may enable reduced sample complexity compared to shadow tomography.

Our simulations compare the potential of different strategies of solving QEI. Blended measurement procedure demonstrates the advantage in high number of measurements setting, and random measurement procedure excels at the low number of measurement setting. On the other hand, classical shadow can not perform properly with the relatively low number of copies used in our simulation.

To extend this research, several directions offer promising prospects. First, although our simulations primarily focused on low-dimensional settings due to hardware limitations, future work can explore higher-dimensional regimes and larger measurement counts. Leveraging increased computational resources and longer simulation periods will help verify whether QEI and the associated procedures maintain stable performance at these expanded scales.

In addition, theoretical approaches to problems related to QEI, such as the original shadow tomography [1] and pretty-good tomography, which relax the success criterion of prediction to achieve linearly scaling in sample complexity [15], can be adapted to QEI and tested in future works. By comparing complexities, sample requirements, and performance trade-offs between these methods on QEI, we may gain valuable insights or refine theoretical bounds, ultimately guiding the development of more practical, scalable quantum event identification techniques.

Finally, integrating machine learning methodologies provides another exciting direction. Techniques like Neural-Shadow Quantum State Tomography (NSQST) [16] and Neural Adaptive Quantum Tomography (NAQT) [17] demonstrate how machine learning can enhance noise resilience, reduce sample complexity, and dynamically optimize measurement strategies. Adopting and adapting these methods in the QEI setting may pave the way for more scalable, robust, and efficient quantum procedures that complement and extend our current findings.

5 Appendix

A The lower bound of the sample complexity of Classical Gapped Shadow Tomography

In this section, we give the proof of the lower bound of Problem 1.7 is $\Omega(\log(m/\delta))$.

Using Theorem A.1, which provides the sample complexity required to distinguish between two distributions, we treat the thresholds $\text{Tr}[M_i\rho] > c$ and $\text{Tr}[M_i\rho] < c - \epsilon$ in classical gapped shadow tomography 1.7 as distinct distributions. This interpretation directly leads to the derivation of the sample complexity for predicting a single measurement outcome.

Theorem A.1 (distinguishing two distributions, [18]). *Successfully distinguishing between two distributions p, q with probability $\geq 1 - \Delta$ requires $\Theta(d_H^2(p, q)^{-1} \log(1/\Delta))$ samples. $d_H^2(p, q)$ is the Squared Hellinger distance between p and q defined as*

$$d_H^2(p, q) = \frac{1}{2} \sum_{i \in [n]} (\sqrt{p_i} - \sqrt{q_i})^2 = 1 - \sum_{i \in [n]} \sqrt{p_i q_i}$$

Lemma A.2 formalizes the sample complexity of prediction for a single measurement outcome, laying the groundwork for further proofs.

Lemma A.2. *Given an unknown diagonal density matrix ρ and a diagonal measurements M , along with real constant values $\epsilon, c \in [0, 1]$, assume that we are promised that either $\text{Tr}[M\rho] \geq c$ or $\text{Tr}[M\rho] \leq c - \epsilon$. We can discern which case it is with a success rate $1 - \Delta$ with $c = \Theta(\log(1/\Delta))$ copies.*

Proof. As ρ, M are diagonal, the best way to discern the cases is to measure ρ with M and getting the probability distribution $(\text{Tr}[M\rho], 1 - \text{Tr}[M\rho])$. By Theorem A.1, since d_H is constant, to distinguish the two distributions $p = (c, 1 - c)$ and $q = ((c - \epsilon), 1 - (c - \epsilon))$ with a success rate $1 - \Delta$, $c = \Theta(\log(1/\Delta))$ copies are sufficient and necessary. \square

Next, building on Lemma A.2, we give a lower bound of the sample complexity of Problem 1.7 with classical input in Theorem A.3.

Theorem A.3 (The Lower Bound of Classical Gapped Shadow Tomography). *We need $k = \Omega(\log(m/\delta))$ copies of ρ to solve Problem 1.7 with a success probability of $1 - \delta$.*

Proof. Assume the unknown state is

$$\rho = \rho_1 \otimes \cdots \otimes \rho_m,$$

where each ρ_i are either $\frac{1}{3}|0\rangle\langle 0| + \frac{2}{3}|1\rangle\langle 1|$ or $\frac{2}{3}|0\rangle\langle 0| + \frac{1}{3}|1\rangle\langle 1|$, and the measurements are

$$M_i = I^{\otimes(i-1)} \otimes |0\rangle\langle 0| \otimes I^{\otimes(m-i)}.$$

Since $\{M_i\}$ commute with each other, the measurement outcomes of each M_i are independent from each other. Therefore, with k copies, the probability that we correctly classify M_i is

$$(1 - \Delta)^m \geq 1 - \delta.$$

Taking the natural logarithm of both sides we get

$$m \log(1 - \Delta) \geq \log(1 - \delta).$$

Using Taylor expansion for small Δ and small δ , we obtain the approximation:

$$-m\Delta \geq -\delta.$$

Rearranging this inequality gives:

$$\Delta \leq \frac{\delta}{m}.$$

Since the sample complexity of prediction for a single measurement outcome is $\Theta(\log(1/\Delta))$ by Lemma A.2, we obtain:

$$k = \Omega\left(\log\left(\frac{m}{\delta}\right)\right).$$

□

References

- [1] S. Aaronson, “Shadow tomography of quantum states,” in *Proceedings of the 50th Annual ACM SIGACT Symposium on Theory of Computing (STOC 2018)*, pp. 325–338, ACM, 2018.
- [2] A. B. Watts and J. Bostanci, “Quantum event learning and gentle random measurements,” in *15th Innovations in Theoretical Computer Science Conference (ITCS 2024)*, vol. 287 of *Leibniz International Proceedings in Informatics (LIPIcs)*, pp. 97:1–97:22, Schloss Dagstuhl–Leibniz-Zentrum für Informatik, 2024.
- [3] E. Schrödinger, “Quantisierung als eigenwertproblem,” *Annalen der Physik*, vol. 79, pp. 361–376, 1926.
- [4] J. B. Altepeter, D. F. V. James, and P. G. Kwiat, “Quantum state tomography,” in *Quantum State Estimation* (M. G. A. Paris and J. Řeháček, eds.), vol. 649 of *Lecture Notes in Physics*, pp. 113–145, Springer, 2004.
- [5] C. H. Bennett, G. Brassard, C. Crépeau, R. Jozsa, A. Peres, and W. K. Wootters, “Teleporting an unknown quantum state via dual classical and einstein-podolsky-rosen channels,” *Physical Review Letters*, vol. 70, pp. 1895–1899, March 1993.
- [6] K. Vogel and H. Risken, “Determination of the density matrix via the Wigner function of the light field,” *Physical Review A*, vol. 40, pp. 2847–2849, 1989.
- [7] Z. Hradil, “Quantum-state estimation,” *Physical Review A*, vol. 55, p. R1561, March 1997.
- [8] D. T. Smithey, M. Beck, M. G. Raymer, and A. Faridani, “Measurement of the wigner distribution and the density matrix of a light mode using optical homodyne tomography: Application to squeezed states and the vacuum,” *Physical Review Letters*, vol. 70, p. 1244, March 1993.
- [9] J. Haah, A. W. Harrow, Z. Ji, X. Wu, and N. Yu, “Sample-optimal tomography of quantum states,” *IEEE Transactions on Information Theory*, vol. 63, no. 9, pp. 5628–5641, 2020.
- [10] H.-Y. Huang, R. Kueng, and J. Preskill, “Predicting many properties of a quantum system from very few measurements,” *Nature Physics*, vol. 16, pp. 1050–1057, 2020.
- [11] C. Bădescu and R. O’Donnell, “Improved quantum data analysis,” in *Proceedings of the 53rd Annual ACM SIGACT Symposium on Theory of Computing (STOC 2021)*, pp. 1398–1411, ACM, 2021.
- [12] A. W. Harrow, C. Y.-Y. Lin, and A. Montanaro, “Sequential measurements, disturbance and property testing,” in *Proceedings of the Twenty-Eighth Annual ACM-SIAM Symposium on Discrete Algorithms (SODA 2017)*, pp. 1598–1611, Society for Industrial and Applied Mathematics, 2017.
- [13] S. Aaronson, “QMA/qpoly \subseteq PSPACE/poly: de-merlinizing quantum protocols,” in *Proceedings of the 21st Annual IEEE Conference on Computational Complexity (CCC 2006)*, (Prague, Czech Republic), pp. 261–273, IEEE, July 2006.
- [14] S. Aaronson, “Quantum copy-protection and quantum money,” in *2009 24th Annual IEEE Conference on Computational Complexity*, (Paris, France), pp. 229–242, IEEE, July 2009.
- [15] S. Aaronson, “The learnability of quantum states,” *Proceedings of the Royal Society A: Mathematical, Physical and Engineering Sciences*, vol. 463, pp. 3089–3114, December 2007.

- [16] V. Wei, W. A. Coish, P. Ronagh, and C. A. Muschik, “Neural-shadow quantum state tomography,” *Physical Review Research*, vol. 6, p. 023250, June 2024.
- [17] Y. Quek, S. Fort, and H. K. Ng, “Adaptive quantum state tomography with neural networks,” *npj Quantum Information*, vol. 7, p. 105, June 2021.
- [18] J. Lee, “Lecture 11: Sublinear algorithms for big data,” 2020. Available at: <https://cs.brown.edu/courses/csci1951-w/lec/lec>